ISSN 2075-3810 (Print), ISSN 2075-3829 (Online)

БІОФІЗИЧНИЙ ВІСНИК, 2025, Вип. 53 BIOPHYSICAL BULLETIN, 2025, Iss. 53

BIOPHYSICAL METHODS

Original article
https://doi.org/10.26565/2075-3810-2025-53-04

UDC 577.359

OPTICAL AND ELECTRON MICROSCOPY IMAGING OF MODEL CIRCULATING TUMOUR CELLS

M. Olenchuk[1,*], G. Monastyrskyi[1], O. Gnatyuk[1], A. Boisen[2], Z. Zhang[2], G. Solyanik[3], D. Kolesnyk[3], S. Karakhim[4], G. Dovbeshko[1]

[1]Department of Physics of Biological Systems, Institute of Physics, NAS of Ukraine, 46 Prospect Nauky, 03028 Kyiv, Ukraine;
[2]Department of Health Technology, Technical University of Denmark, Ørsteds Plads, Building 345C, DK-2800 Kgs. Lyngby, Denmark;
[3]Laboratory of Molecular and Cellular Mechanisms of Metastasis, R. E. Kavetsky Institute of Experimental Pathology, Oncology and Radiobiology, NAS of Ukraine, 45 Vasyl'kivs'ka St., 03022 Kyiv, Ukraine;
[4]Department of Muscle Biochemistry, O. V. Palladin Institute of Biochemistry, NAS of Ukraine, 9 Leontovicha Str., 01030 Kyiv, Ukraine
**Corresponding author: m.olenchuk@yahoo.com*
Submitted April 28, 2025; Revised May 25, 2025;
Accepted May 25, 2025

Background: Microscopy is a key tool in biophysical research for visualizing living cells' morphology, structure, and dynamic processes. Depending on the specific research goals, various optical and electron microscopy techniques can be applied, each offering unique benefits. Determining the structural features of the cytoskeleton, nucleus, and membrane of circulating tumor cells in the model Lewis lung carcinoma (LLC) is an important biophysical and biological task, as it will allow identifying targets for antitumor and antimetastatic therapy, as well as investigating the mechanisms of action of antitumor drugs. However, comprehensive multimodal imaging of such cells — particularly under non-adherent conditions — remains limited in the literature due to the difficulty of working with such models.
Objectives: This study aimed to visualize Lewis lung carcinoma (LLC) cells cultured under de-adhesive conditions using various microscopy techniques for their characterization and to examine the cancer cells' structure and functionality. The goal was to evaluate each method's individual capabilities and combined strengths in revealing cellular morphology, internal structure, and nanoparticle interactions.
Materials and Methods: LLC cells were obtained from the National Bank of Cell Lines and Tumor Strains of the IEPOR (NAS of Ukraine) and cultured in RPMI-1640 medium under conditions of de-adhesive growth. Imaging was performed using inverted optical microscopy (Euromex Oxion), fluorescence and confocal microscopy (Carl Zeiss LSM 510) with F-actin (Alexa Fluor 488-phalloidin) and nuclear (Hoechst 33342) staining, and label-free Coherent Anti-Stokes Raman Scattering (CARS) microscopy (Leica TCS SP8). Scanning electron microscopy (TESCAN MIRA3 LMU) was used for high-resolution surface imaging. 2D-MoS_2 nanoparticles, as well as 2D-MoS_2 and doxorubicin simultaneously, were applied to investigate nanoparticle-mediated labeling and cellular uptake.
Results: A comparative analysis of multiple imaging modalities — including optical, fluorescence, confocal, CARS, and SEM — was applied to Lewis lung carcinoma (LLC) cells. Fluorescence microscopy with specific fluorophores made it possible to analyze the size and properties of actin fibers and showed that nuclei occupy most of the deadhesive cells. Electron microscopy revealed numerous filopodia on the cell surface. CARS showed the presence of lipid droplets in the cells.

Citation: Olenchuk M, Monastyrskyi G, Gnatyuk O, Boisen A, Zhang Z, Solyanik G, Kolesnyk D, Karakhim S, Dovbeshko G. Optical and electron microscopy imaging of model circulating tumour cells. Biophysical Bulletin. 2025;53:46–59. https://doi.org/10.26565/2075-3810-2025-53-04

Conclusions: Each microscopy method provided complementary insights into cell morphology, cytoskeletal organization, lipid content, and surface ultrastructure. Nanoparticles demonstrated high utility as dual imaging and therapeutic agents. This work represents the first detailed SEM study of non-adherent LLC cells and highlights the potential of integrated multimodal imaging for studying circulating tumor cell models.
KEY WORDS: model circulating tumour cells LLC; SEM; CARS; confocal microscopy; nanoparticles.

Microscopy imaging techniques are widely utilized for studying dynamic cellular behavior in biophysics, enabling precise and real-time analysis of a broad range of cellular and tissue parameters. It allows for the observation of intercellular interactions, the behavior of individual cells, cytoskeletal dynamics, the activity of cellular organelles and molecules, and the measurement of cell proliferation over time. Various imaging modalities can be applied, including phase-contrast microscopy [1], fluorescence and confocal microscopy [1], multiphoton microscopy [2, 3], stimulated emission depletion microscopy (STED) [4], scanning electron microscopy (SEM) [5], and transmission electron microscopy (TEM) [6, 7].

Inverted microscopes are frequently employed in research to analyze and study tissues and cells, particularly living cells. Since many cellular processes can be directly visualized under the microscope, different imaging techniques are required depending on the experimental needs. Some experiments, such as chemotaxis assays or tube formation analysis, do not require staining and can be readily visualized using optical microscopy (e.g., phase contrast). However, due to the optical transparency of tissues to visible light and the necessity for sufficient contrast, various staining markers are often employed. Although optical microscopy exhibits low phototoxicity [8], it can still influence cellular behavior and must be minimized. For instance, light exposure should occur only during image acquisition, and the intensity of illumination can be reduced by employing highly sensitive cameras.

Fluorescence microscopy, which utilizes various fluorophores, enables the detection of more structural details and molecular interactions [9]. When applying fluorescence-based techniques, such as confocal microscopy, it is particularly critical to minimize cellular stress caused by excitation light. Phototoxic effects and photobleaching occur rapidly in live cells and can significantly alter experimental outcomes [10]. Stimulated emission depletion microscopy provides a clear view of a cell's cytoskeleton.

Multiphoton microscopy offers several advantages for live-cell imaging. The use of longer excitation wavelengths substantially reduces photobleaching compared to single-photon confocal imaging, thus enhancing cell viability during prolonged observation periods. This technique also enables three-dimensional (3D) fluorescent imaging of live cells at depths of several hundred micrometers in thick, highly scattering samples [11].

Coherent anti-Stokes Raman scattering (CARS) microscopy has been increasingly utilized by cell biologists to study the dynamics of living cells with chemical specificity in a non-invasive, label-free manner [12–15]. Most CARS-based studies in cell biology have focused on lipid dynamics [12, 16], as CARS signals strongly from the C-H bond stretching vibrations in lipids. In fluorescence microscopy, achieving stable lipid-specific labeling remains challenging due to the interference of labeling processes with lipid function and localization. Consequently, in live-cell studies, performing rapid experiments on lipids and lipid droplets while maintaining quantitative accuracy is extremely difficult [17]. CARS microscopy has thus proven to be an excellent technique for investigating lipid dynamics in living cells with high chemical specificity.

The electron beam within a transmission electron microscope (TEM) poses significant challenges for biological specimens due to its high energy. To penetrate the sample and exit from the opposite side, the beam must possess sufficient energy, which can lead to local temperatures exceeding 100 °C where it strikes the specimen. Although scanning electron

microscopes (SEMs) employ lower-energy electron beams, they can still cause damage to biological samples. Additionally, the vacuum environment inside the microscope promotes water evaporation from biological samples, further complicating imaging. Therefore, careful sample preparation is crucial. SEM is particularly well-suited for analyzing cell morphology, proliferation, metabolism, and expression profiles.

Fluorescence confocal microscopy is widely employed for the investigation of Lewis lung carcinoma (LLC) cells. Depending on the specific objectives of the study, various fluorescent dyes are utilized. Green fluorescent protein (GFP) is commonly used for monitoring cell division, migration, and intercellular interactions [18]. Carboxyfluorescein succinimidyl ester (CFSE) is frequently applied in immunological assays to assess lymphocyte proliferation and migration [19]. The red fluorescent protein Katushka [20] has been used in LLC studies; however, its variable expression levels within cell cultures present technical challenges when attempting to image cells with both high and low fluorescence intensities in the same field of view. Hoechst 33342 is routinely used for nuclear staining, cell cycle analysis, and apoptosis evaluation [21]. For cytoskeletal studies, phalloidin conjugates are applied, including far-red Alexa Fluor 633 phalloidin, which specifically stains the actin cytoskeleton [22], as well as Alexa Fluor 488 (green) and Alexa Fluor 546 (orange) phalloidin for precise visualization of filamentous actin (F-actin) structures [23].

The radiobiological response of Lewis lung carcinoma cells treated with gold nanoparticles was examined in [24], where scanning electron microscopy was employed for visualization. Samples were polymerized, and ultrathin sections (approximately 100 nm) were obtained using a diamond knife. These sections were stained with uranyl acetate and lead citrate, and imaged using a FEI Nova NanoSEM 230 in scanning transmission electron microscopy (STEM) mode at 15 kV in bright field vacuum conditions.

In this work, we present integrated data from optical and electron microscopy of circulating tumor cells (CTCs), which serve as a model for circulating metastatic cells. We assess the capabilities of each imaging modality independently and in combination. Using confocal microscopy with Alexa Fluor 488-conjugated phalloidin and Hoechst 33342, we aimed to analyze potential cytoskeletal reorganization and distinctive features in F-actin architecture in non-adherent LLC cells compared to their adhesive counterparts, as previously reported in [14]. The application of two-dimensional molybdenum disulfide (2D-MoS_2) nanoparticles as a substitute for conventional fluorescent dyes in confocal microscopy represents a promising alternative and warrants further investigation. Model deadhesive LLC cells have not been studied previously, and both electron images of deadhesive cells and confocal images characterizing actin fibers in such cells are absent in literature.

MATERIALS AND METHODS

Cell culture

Lewis lung carcinoma cells (LLC) were obtained from the National Bank of Cell Lines and Tumor Strains of the IEPOR (R. E. Kavetsky Institute of Experimental Pathology, Oncology, and Radiology) of the National Academy of Sciences of Ukraine [25]. Cells were maintained under standard in vitro conditions at 37 °C in a humidified atmosphere containing 5% CO_2. Cultures were grown in RPMI 1640 medium (Sigma-Aldrich) supplemented with 10% fetal calf serum (FCS), 2 mM L-glutamine, and 40 μg/mL gentamicin to prevent bacterial contamination. For experimental procedures, LLC cells were seeded at a density of 0.3×10^6 cells per 60 mm Petri dish. To investigate de-adhesive growth conditions, Petri dishes were left pre-coated with poly-2-hydroxyethyl methacrylate (poly-HEMA) solution. Poly-HEMA coating prevents cell attachment by forming a hydrophilic, non-adhesive surface, thus allowing

the study of de-adhesive cell behavior and morphology [14]. After seeding, cells were incubated for three days without changing the medium to maintain stable experimental conditions and to allow for natural progression of growth and morphological adaptation.

Method of preparation-of 2D-MoS_2 is dispersant-free liquid exfoliation of solvent-free mechanochemically delaminated bulk MoS_2 developed at the L. V. Pisarzhevsky Institute of Physical Chemistry of the National Academy of Sciences of Ukraine by Dr. Oleg Posudievsky [26]. The initial concentration of the nanoparticle suspension was 0.15 mg/mL.

To investigate the biological effects of 2D-MoS_2 on tumor cells, 225 μL of the nanoparticle suspension was added to 1275 μL of cell culture medium in which Lewis lung carcinoma cells were maintained. Cells were cultured in 35 mm Petri dishes for 24 hours under standard incubation conditions (37 °C, 5% CO_2, humidified atmosphere). This dilution yielded a final concentration of 2D-MoS_2 nanoparticles of 0.021 mg/mL in the culture medium.

In a separate experimental group, doxorubicin (DOX) was added to the medium containing nanoparticles at 0.05 mg/mL concentration. The amount of doxorubicin added was standardized at 100 μL per 10,000 cells, based on initial seeding density. This setup allowed the evaluation of combined MoS_2 and DOX influence on the cells.

For control experiments, LLC cells were incubated under identical conditions, using the same culture medium and time frame, but without the addition of nanoparticles or doxorubicin. These controls were used to assess baseline cellular morphology, viability, and fluorescence without external agents.

Optical Microscopy

Optical imaging of the LLC cells was performed using an inverted microscope, Euromex Oxion Inverso (model OX.2453-PLPHF, Euromex Microscopen, The Netherlands). Imaging was conducted at 400× total magnification using phase contrast mode to enhance visualization of cellular morphology under live, unstained conditions. Optical observations provided preliminary assessments of cell proliferation patterns, morphology, and behavior under different substrate adhesion conditions.

Scanning Electron Microscopy (SEM)

High-resolution morphological characterization of the LLC cells was carried out using a TESCAN MIRA LMU scanning electron microscope equipped with a Schottky field emission cathode. Secondary electron imaging mode was employed to optimize surface topography visualization. A contrast-optimized acceleration voltage of 10.0 kV was applied, with an imaging field of view set at 50 μm, yielding a final total magnification of approximately 3,790×. Samples were fixed, dehydrated through graded ethanol series, dried, and sputter-coated with a thin gold layer (~20 nm) before SEM analysis to ensure electrical conductivity and prevent charging artifacts.

Sample Preparation for Scanning Electron Microscopy

Preparation of biological samples for scanning electron microscopy (SEM) requires a series of critical and meticulous steps to preserve cellular morphology and prevent artifacts. In this study, Lewis Lung Carcinoma (LLC) cells were cultured for 48 hours in Petri dishes pre-coated with poly (2-hydroxyethyl methacrylate) (poly-HEMA), a polymer that prevents cell adhesion to the substrate, thereby promoting a suspension-like growth state.

Following incubation, the cell suspension was gently harvested by low-speed centrifugation (1000 rpm for 5 minutes) to minimize mechanical stress and aggregation. The cell pellet was immediately fixed in a solution containing 4% paraformaldehyde and 2.5%

glutaraldehyde in phosphate-buffered saline (PBS), ensuring stabilization of cellular structures at the ultrastructural level.

Subsequent triple washing with PBS and two additional washes with distilled water were performed to thoroughly remove residual salts, a crucial step to prevent salt crystallization artifacts during the drying process. Fixed cell suspensions were then deposited onto polished silicon wafers, chosen for their smooth, conductive surface and chemical inertness. Samples were air-dried in a laminar flow hood to gently remove moisture while preserving cell morphology. To ensure adequate charge dissipation during SEM imaging, a conductive gold layer approximately 20 nm thick was applied to the sample surface by magnetron sputtering.

Coherent Anti-Stokes Raman Scattering (CARS) and Second Harmonic Generation (SHG) Microscopy

CARS and SHG imaging were performed using a Leica TCS SP8 CARS microscope (Leica Microsystems, Germany). This multimodal system allows simultaneous acquisition of vibrational (CARS) and structural (SHG) signals without the need for exogenous labeling. Imaging was conducted with constant excitation parameters: pump and Stokes beam powers at the sample were maintained at 1 W, with the system output power measured at 870 mW. The spectral acquisition was tuned to optimize sensitivity for lipid structures, exploiting the high C-H vibrational contrast in the cellular environment. This approach enabled non-invasive visualization of lipid-rich compartments such as membranes and lipid droplets, critical for understanding cell morphology and metabolism under various conditions.

Confocal Laser Scanning Microscopy

Confocal fluorescence imaging of the LLC cells was conducted using an LSM 510 confocal laser scanning microscope (Carl Zeiss, Germany). Fluorescence detection utilized FSet10wf and FW1-2: FSet20wf filter sets optimized for capturing emission from common fluorophores under UV lamp and laser excitation. All images were acquired using an LD Plan-Neofluar 40x/0.6 Korr objective lens, ensuring high-resolution imaging with minimal spherical aberration. Confocal microscopy allowed three-dimensional reconstruction of cellular structures, and provided complementary information on intracellular organization, particularly under de-adhesive conditions where cytoskeletal rearrangements and lipid droplet formation are prominent.

RESULT AND DISCUTION

SEM Imaging

For detailed morphological analysis of LLC cells, secondary electron imaging was performed using a field-emission scanning electron microscope under optimized conditions. The use of secondary electrons enabled high-resolution visualization of surface features with enhanced topographical contrast. Notably, due to the presence of a robust cytoskeletal network, the LLC cells displayed sufficient mechanical stability to withstand electron beam exposure without notable structural collapse.

The Fig. 1. shows representative SEM images with subsequent magnification of the same spot.

Dense clusters of spherical cells without signs of spreading or flattening are observed in the centre and upper right regions of the image. Cells have maintained their rounded morphology, characteristic of suspension growth, with clearly defined and textured surface features. Groupings of cells into small colonies are apparent, likely due to residual intercellular contacts or aggregation following centrifugation.

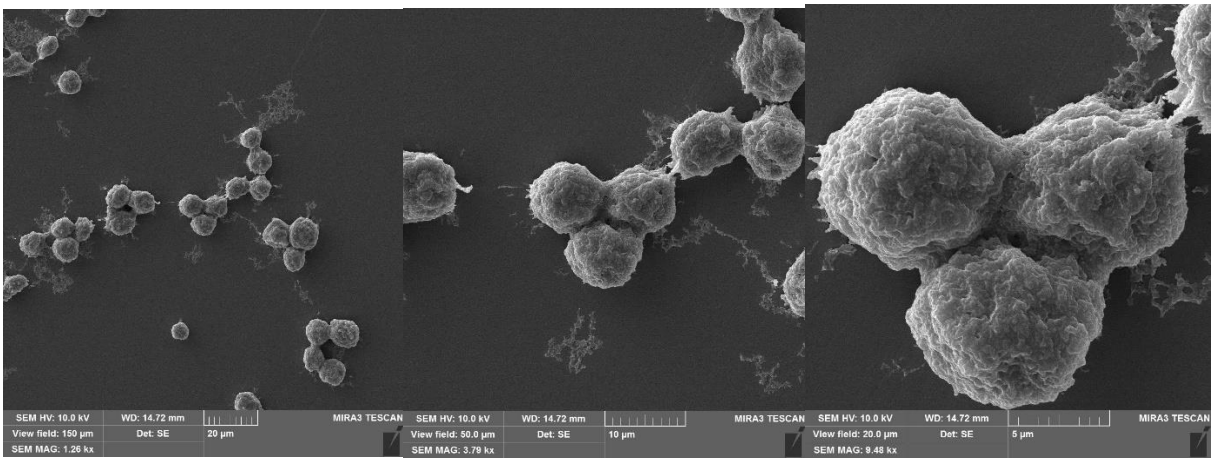

a scale 20 µm b scale 10 µm c scale 5 µm

Fig. 1. Representative SEM images of LLC cells cultured under de-adhesive conditions:
a) Low magnification (1260X, scale bar = 20 µm, field of view 150 µm) showing dispersed spherical cells and small aggregates on the polished silicon wafer substrate;
b) Intermediate magnification (3790X, scale bar = 10 µm, field of view 50 µm) revealing detailed cell contours and extracellular filamentous material;
c) High magnification (9480X, scale bar = 5 µm, field of view 20 µm) displaying individual cells with rugged membrane surfaces featuring microprotrusions and vesicular structures, suggestive of active surface remodelling.

The cell surfaces appear heterogeneous, exhibiting numerous microvilli, blebs, and micropseudopodia, indicative of active membrane processes. These features may reflect apoptotic changes or stress responses induced by the non-adhesive culture environment. The SEM analysis of LLC cells, cultured under non-adhesive conditions and fixed in suspension, confirms the preservation of their spherical morphology and the presence of dynamic surface structures. This model system provides valuable insights for simulating the behavior of CTCs and investigating adhesion-independent morphological adaptations.

CARS and SHG Imaging

CARS and SHG images of de-adhesive LLC cell cultures are presented in Figure 2. For CARS imaging of the cell, forward-detected signals (F-CARS) were collected to enhance signal-to-noise ratio and achieve high-resolution vibrational contrast.

During CARS acquisition, the frequency difference between the pump (ω_p) and Stokes (ω_s) beams was tuned to specific Raman-active vibrational modes. The first setting targeted 1650 cm^{-1}, corresponding to the Raman shift associated with the C=C [27], which matches the Raman shift of symmetric stretching vibration CH_2 (by the way, the strongest vibration belongs to asymmetric CH_2 near 2930 cm^{-1} in CARS and 2937 cm^{-1} in Raman spectra [14, 28]), predominantly originating from lipid-rich cellular compartments such as membranes and lipid droplets.

Figure 2 displays representative F-CARS and SHG images acquired at these vibrational frequencies. The 1650 cm^{-1} imaging (Fig. 2a) emphasizes regions rich in unsaturated lipids and proteins [27], providing insight into the biochemical organization of the cells. Imaging at 2850 cm^{-1} (Fig. 2c) highlights the distribution of saturated lipid structures [28], which are critical for membrane integrity and cellular energy storage. Additionally, SHG signals were simultaneously collected to visualize non-centrosymmetric structures, such as collagen fibers or ordered membrane regions, without the need for exogenous labeling as well non-resonance background.

The combination of F-CARS and SHG imaging thus offers a powerful, label-free approach to assess both the molecular composition and structural organization of LLC cells under de-adhesive conditions

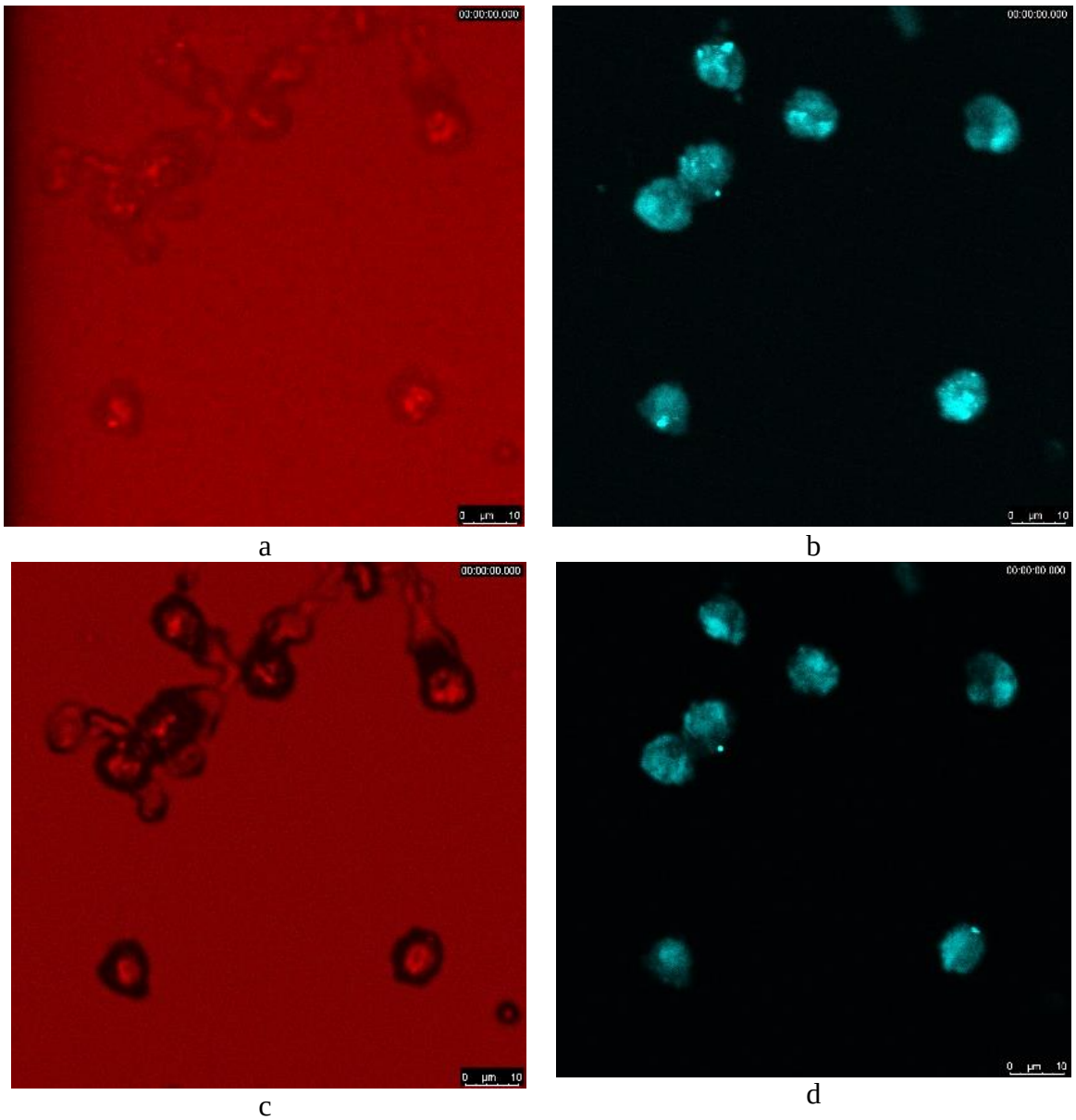

Fig. 2. F-CARS (a) and SHG (b) images at 1650 cm^{-1}; F-CARS (c) and SHG (d) images at 2850 cm^{-1} of de-adhesive LLC. Scale bar = 10 μm.

F-CARS imaging revealed distinct vibrational contrast between content-rich and content-poor regions within de-adhesive LLC cells. Content-rich cellular poles, comprising the cell membrane along with associated lipid droplets, exhibited a strong CARS signal due to the high density of CH_2 groups and unsaturated lipid components. In contrast, content-poor poles, consisting primarily of the cell membrane with minimal internal lipid accumulation, produced a significantly weaker CARS signal. This variation in CARS intensity provides valuable biochemical information about intracellular heterogeneity and lipid distribution under non-adherent growth conditions.

Optical Imaging

Living mammalian cells are nearly as translucent as ice cubes submerged in water. Consequently, to render them visible under standard brightfield or fluorescence microscopy, cells must be either stained or genetically modified to absorb, emit, or scatter light effectively. Staining enables the differentiation of cells and the visualization of specific intracellular structures. Among various staining techniques, immunofluorescence represents the gold standard, wherein specific antibodies conjugated with fluorescent dyes bind to target proteins within the cell. This method provides enhanced contrast and allows simultaneous detection and localization of multiple proteins through the use of differently colored fluorophores.

To study the cytoskeletal structure and the organization of filamentous actin (F-actin) and the nucleus in LLC cells, the dyes Alexa Fluor 488-conjugated phalloidin and Hoechst 33342 were used, respectively. An image of cells stained with Alexa Fluor 488-conjugated phalloidin obtained using an inverted microscope is shown in Figure 3a, while the corresponding confocal image of the same sample is presented in Figure 4a. LLC cells stained with Hoechst 33342 are shown in Figures 3b and 4b.

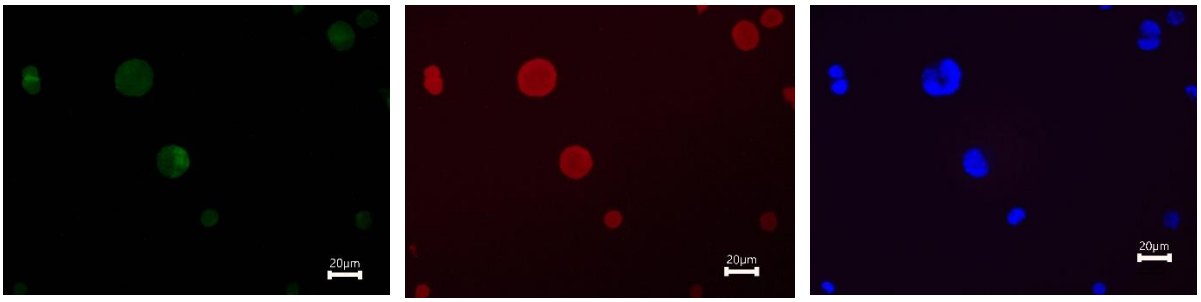

a b c

Fig. 3. Inverted microscope images of F-actin staining LLC cells, cell nuclei stained by Hoechst 33342.2. Scale bar = 20 μm.

Fluorescence microscopy was employed to gain more detailed information on intracellular structures and molecular dynamics. A standard set of three fluorescence filter cubes — targeting blue (DAPI channel, ~460 nm emission), green (FITC channel, ~520 nm emission), and red (Texas Red or TRITC channel, ~620 nm emission) — was utilized to visualize different cellular components selectively. The blue filter typically highlights nuclei stained with DAPI or similar dyes, the green filter reveals cytoskeletal structures or membrane components labeled with FITC, and the red filter is commonly used to detect actin filaments or lipid structures stained with TRITC or analogous fluorophores.

In our experiment, it is clearly observed that the cells exhibit a de-adhesive phenotype, as indicated by their rounded morphology. A heterogeneous distribution of F-actin within the cell is also well visualized (Fig. 3a), along with distinct chromatin organization features within the nucleus (Fig. 3c). However, in the case of our specific optical system, image quality was reduced during digital conversion, primarily due to the limited performance of the CCD camera used. Confocal fluorescence microscopy was employed to visualize cytoskeletal organization and nuclear morphology in de-adhesive LLC cells. Representative confocal images are presented in Figure 4. The green fluorescence channel was selectively enhanced to emphasize the staining of filamentous actin (F-actin) using Alexa Fluor 488-conjugated phalloidin (Fig. 4a). Simultaneously, cell nuclei were counterstained with Hoechst 33342, a DNA-specific dye that emits in the blue channel (Fig. 4b).

In de-adhesive LLC cells, F-actin fibers formed prominent perinuclear structures, tightly encircling the nuclei. This arrangement is similar to that observed in cells grown under adhesive conditions [14]; however, in de-adhesive cells, the F-actin fibers exhibited reduced diameter

and shortened length. These observations suggest that cytoskeletal remodeling occurs in response to the absence of adhesion forces, leading to a more compact and mechanically adapted cytoskeletal architecture. The combined use of F-actin and nuclear staining thus provided detailed insights into the structural adaptations of LLC cells under de-adhesive culture conditions (Fig. 4c).

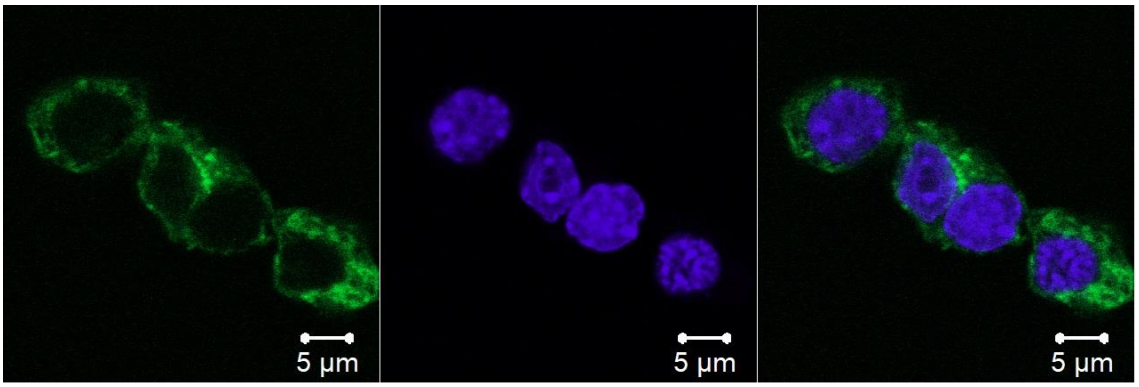

a b c

Fig. 4. Confocal images of F-actin staining (a) in LLC cells under de-adhesive growth, cell nuclei stained by Hoechst 33342.2 (b) and (c) image from both channels. Scale bar = 5 µm.

This multicolor imaging approach provided complementary datasets that enabled precise analysis of both the general morphology and the specific intracellular organization of LLC cells.

However, it is important to acknowledge that such invasive preparative techniques can significantly alter cellular behavior, thereby compromising the in vivo relevance of in vitro live-cell observations. The chemical or photonic stress introduced during sample staining and preparation can lead to artifacts that obscure native physiological states.

Nanoparticles can be effectively employed as contrast agents for enhancing fluorescence signals during confocal microscopy imaging of cells. In this study, an aqueous suspension of two-dimensional molybdenum disulfide (2D-MoS_2) nanoparticles was used to investigate their interaction with LLC cells and to assess their potential as imaging enhancers.

Figure 5 presents representative confocal images of three experimental groups: control LLC cells (Fig. 5a), LLC cells incubated with MoS_2 nanoparticles (Fig. 5b), and LLC cells treated with a doxorubicin and MoS_2 nanoparticle (Fig. 5c).

For fluorescence excitation, lasers of different wavelengths were employed to selectively stimulate various components: 543 nm laser (T1, 60% intensity) was used for excitation of the red fluorescence channel, 488 nm laser (T2, 50% intensity) was used for excitation of the green fluorescence channel, 405 nm laser (T3, 30% intensity) was used for excitation of the blue fluorescence channel.

Beam splitters FW1-1 (FSet10wf) and FW1-2 (FSet20wf) were applied according to the corresponding fluorescence sets. Additionally, ultraviolet (UV) excitation was performed in transmission mode without emission filters to detect the autofluorescence of cells and nanoparticles.

Visualization of LLC cells (Fig. 6 a, d), LLC cells incubated with 2D-MoS_2 nanoparticles (Fig. 6 b, e) was also performed under widefield illumination conditions. Figure 6 presents images acquired using both halogen lamp excitation in transmission mode and ultraviolet (UV) lamp excitation with selective optical filtering with FSet10 wf and FSet20 wf filters.

The application of 2D-MoS_2 nanoparticles with the anticancer drug doxorubicin resulted in extensive fluorescence labeling of LLC cells, as demonstrated in Figure 5c and Figure 6 c, f. Confocal imaging revealed uniform staining of the entire cell body within the green

fluorescence range, accompanied by pronounced luminescence signals in both the green and red spectral regions.

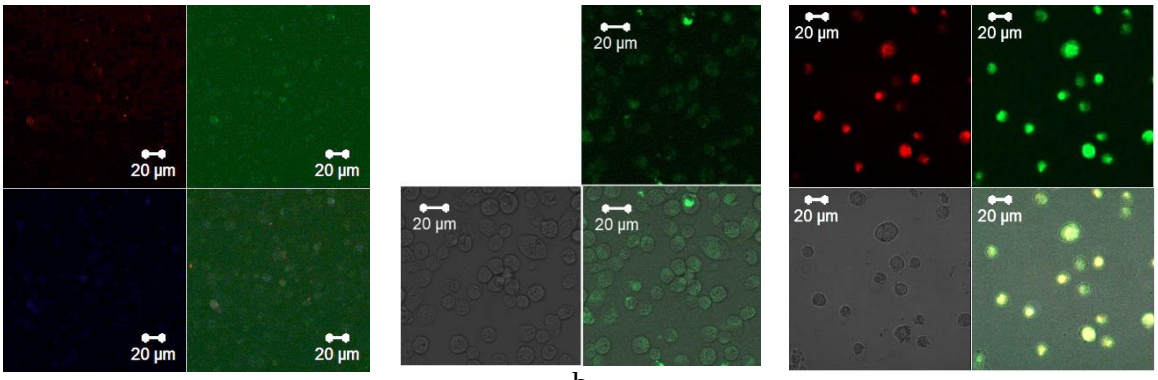

Fig. 5. Confocal images of LLC cells (a), LLC cells with 2D-MoS_2 nanoparticles (b), LLC cells with 2D-MoS_2 nanoparticles with doxorubicine (c). excitation: Laz 543 nm (a, c), 488 nm (a, b, c), 405 nm (a), transmission mode (b, c). Scale bar = 20 µm.

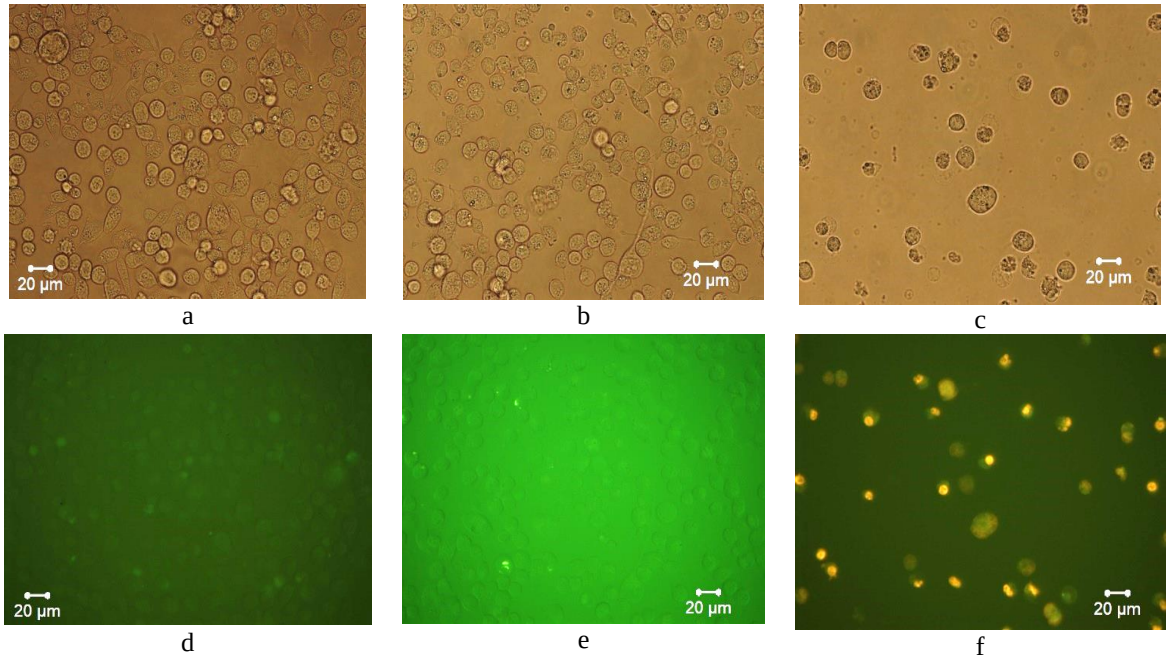

Fig. 6. Confocal images of LLC cells (a), LLC cells with 2D-MoS_2 nanoparticles (b), LLC cells with 2D-MoS_2 nanoparticles with doxorubicine (c) with a halogen lamp excitation, transmittance mode; and LLC cells (d), LLC cells with 2D-MoS_2 nanoparticles (e), LLC cells with 2D-MoS_2 nanoparticles with doxorubicine (f) with UV lamp excitation with FSet10 wf and FSet20 wf filters. Scale bar = 20 µm.

Our results indicate that 2D nanoparticles can be effectively utilized as multifunctional markers for the visualization of cellular structures (Fig. 5 b, 6 b, e). Specifically, they facilitate the detection of critical cellular events such as apoptosis, necrosis, and intracellular redistribution of therapeutic agents like DOX. Importantly, MoS_2 nanoparticles alone did not exhibit cytotoxic effects on LLC cancer cells; instead, a modest increase in proliferative activity was observed, suggesting a degree of cellular tolerance to the nanomaterial.

We supposed that the MoS_2 particles may break down and easy split in aggressive environment of tumor cells during long-term incubation (1 days) and convert to nanometer-sized MoS_2 nanoparticles (referred to as "dots") successfully entered the cells (Fig. 5b), localizing predominantly within the cytoplasm and often accumulating in close proximity to

the nucleus. In cells treated with the 2D-MoS_2 and DOX, the nanoparticles, together with the doxorubicin, appeared to permeate the intracellular space extensively, covering both perinuclear and cytoplasmic regions and effect of staining became better.

Moreover, cells seeded onto nanostructured gold surfaces and treated with DOX and 2D-MoS_2-exhibited enhanced fluorescence intensity under ultraviolet excitation when using a red emission filter. This effect is likely due to the plasmonic properties of the gold substrate, which can amplify local electromagnetic fields and thereby increase the fluorescence signal of nearby molecules.

Overall, our findings suggest that 2D-MoS_2 nanoparticles, particularly when combined with nanostructured gold surfaces, hold promise as potent contrast enhancers in confocal microscopy and as luminescent markers operating effectively in both green and red spectral regions.

CONCLUSION

In this study, we demonstrated that two-dimensional molybdenum disulfide (2D-MoS_2) nanoparticles can serve as effective markers for cell structure visualization and for enhancing image contrast in fluorescence microscopy. The use of 2D-MoS_2 nanoparticles enabled strong and broad fluorescence signals in the green and red spectral ranges without the need for additional staining, offering a less invasive alternative for live-cell imaging.

Scanning electron microscopy (SEM) was shown to be a powerful technique for detailed morphological characterization of Lewis lung carcinoma (LLC) cells. SEM provided high-resolution imaging of cell surfaces and membrane features, revealing abundant filopodia structures on their surfaces. However, it requires a specific and carefully controlled sample preparation protocol, including fixation, dehydration, and conductive coating, to prevent sample damage and charging under the electron beam.

The advantages of Coherent Anti-Stokes Raman Scattering (CARS) microscopy were also highlighted in this work. CARS offers a non-invasive, label-free approach to study live cells with chemical specificity. CARS microscopy confirmed the presence of lipid droplets within the cytoplasm. By tuning the frequency difference between the pump and Stokes beams, it was possible to selectively visualize different cellular components. Imaging at 1650 cm^{-1} targeted the cis C=C stretch vibrations characteristic of unsaturated lipids and the Amide I band associated with protein structures, while imaging at 2850 cm^{-1} highlighted symmetric CH_2 stretch vibrations, predominantly from lipid-rich domains. The ability of CARS to distinguish between lipid and protein content without external markers underscores its potential for studying cellular dynamics with minimal perturbation.

Overall, the combination of advanced microscopy techniques, including SEM, CARS, confocal fluorescence microscopy, and nanoparticle-assisted imaging, provides a comprehensive toolkit for investigating the morphology, molecular composition, and dynamic behavior of cancer cells under different culture conditions. Undoubtedly, high-resolution visualization of such cells provides deeper insights into the biophysical and biochemical mechanisms underpinning metastatic dissemination.

ACKNOWLEDGMENTS

This work is supported by project NRFU № 2021.01/0229 “Biophysical characteristics of circulating metastatic cells as potential targets of antimetastatic therapy” (2022-2025). We express our gratitude to Doctor of Chemical Sciences, Senior Researcher O. Yu. Posudievsky for providing aqueous suspensions of molybdenum disulfide.

CONFLICT OF INTEREST

The authors declare that there is no conflict of interest.

Authors' ORCID ID

Maryna Olenchuk https://orcid.org/0000-0002-3710-6349
Grygorii Monastyrskyi https://orcid.org/0000-0002-4910-552X
Olena Gnatyuk https://orcid.org/0000-0003-4406-5503
Anja Boisen https://orcid.org/0000-0002-9918-6567
Zhongyang Zhang https://orcid.org/0000-0002-9035-2880
Galina Solyanik https://orcid.org/0000-0002-8657-1263
Denis Kolesnik https://orcid.org/0000-0002-1223-3544
Sergiy Karakhim https://orcid.org/0000-0002-8389-0584
Galyna Dovbeshko https://orcid.org/0000-0002-7701-0106

REFERENCES

1. Zuluaga AF, Drezek R, Collier T, Lotan R, Follen M, Richards-Kortum R. Contrast agents for confocal microscopy: how simple chemicals affect confocal images of normal and cancer cells in suspension. J Biomed Opt. 2002;7(3):398–403. https://doi.org/10.1117/1.1481047
2. Torcellan T, Stolp J, Chtanova T. In vivo imaging sheds light on immune cell migration and function in cancer. Front Immunol. 2017:8;309. https://doi.org/10.3389/fimmu.2017.00309
3. Perrin L, Bayarmagnai B, Gligorijevic B. Frontiers in intravital multiphoton microscopy of cancer. Cancer Rep. 2020;3:e1192. https://doi.org/10.1002/cnr2.1192
4. Hein B, Willig KI, Hell SW. Stimulated emission depletion (STED) nanoscopy of a fluorescent protein-labeled organelle inside a living cell. Proc Natl Acad Sci USA. 2008;105(38):14271–6. https://doi.org/10.1073/pnas.0807705105
5. Ali R, El-Boubbou K, Boudjelal M. An easy, fast and inexpensive method of preparing a biological specimen for scanning electron microscopy (SEM). MethodsX. 2021;8:101521. https://doi.org/10.1016/j.mex.2021.101521
6. Peckys DB, Mazur P, Gould KL, de Jonge N. Fully hydrated yeast cells imaged with electron microscopy. Biophys J. 2011;100(10):2522–9. https://doi.org/10.1016/j.bpj.2011.03.045
7. Hou WL, Chang M, Liu XF, Hu LS, Hua SC. Proteomic and ultrastructural analysis of Clara cell and type II alveolar epithelial cell-type lung cancer cells. Transl Cancer Res. 2020;9(2):565–76. https://doi.org/10.21037/tcr.2019.12.04
8. Conchello JA, Lichtman JW. Optical sectioning microscopy. Nat Methods. 2005;2(12):920–31. https://doi.org/10.1038/nmeth815
9. Cook A, Walterspiel F, Deo C. HaloTag-based reporters for fluorescence imaging and biosensing. Chembiochem. 2023;24(12):e202300022. https://doi.org/10.1002/cbic.202300022
10. Khodjakov A, Rieder CL. Imaging the division process in living tissue culture cells. Methods. 2006;38(1):2-16. https://doi.org/10.1016/j.ymeth.2005.07.007
11. Rubart M. Two-photon microscopy of cells and tissue. Circ Res. 2004;95(12):1154–66. https://doi.org/10.1161/01.RES.0000150593.30324.42
12. Nahmad-Rohen A, Regan D, Masia F, McPhee C, Pope I, Langbein W, et al. Quantitative label-free imaging of lipid domains in single bilayers by hyperspectral coherent raman scattering. Anal. Chem. 2020;92(21):14657–66. https://doi.org/10.1021/acs.analchem.0c03179
13. Shi J, Bera K, Mukherjee P, Alex A, Chaney EJ, Spencer-Dene B, et al. Weakly supervised identification and localization of drug fingerprints based on label-free hyperspectral CARS microscopy. Anal Chem. 2023;95(29):10957–65. https://doi.org/10.1021/acs.analchem.3c00979
14. Gnatyuk O, Kolesnyk D, Voitsitskyi T, Karakhim S, Nikolenko A, Dementjev A, et al. Vibrational markers of a model circulating metastatic cells LLC-R9. Spectroscopy Journal. 2024;2(4):306–21. https://doi.org/10.3390/spectroscj2040018
15. Dovbeshko G, Gnatyuk O, Dementjev A, Rutkauskas D, Kovalska E, Baldycheva A, et al. Coherent anti-stokes Raman scattering spectroscopy (CARS) and imaging of DNA on graphene layers and glass covers. FlatChem. 2021;27:100243. https://doi.org/10.1016/j.flatc.2021.100243
16. Pezacki JP, Blake JA, Danielson DC, Kennedy DC, Lyn RK, Singaravelu R. Chemical contrast for imaging living systems: molecular vibrations drive CARS microscopy. Nat Chem Biol. 2011;7:137–45. https://doi.org/10.1038/nchembio.525
17. Liu C, He S, Guo XF, Wang H. A novel near-infrared AIE probe for sensitive imaging of lipid droplet and dual-parameter cancer diagnosis. Anal Chim Acta. 2025;1352:343916. https://doi.org/10.1016/j.aca.2025.343916

18. Rashidi B, Moossa AR, Hoffman RM. Specific route mapping visualized with GFP of single-file streaming contralateral and systemic metastasis of Lewis lung carcinoma cells beginning within hours of orthotopic implantion. J Cell Biochem. 2013;114:1738–43. https://doi.org/10.1002/jcb.24516
19. Lin T, Liao Y, Chang W, Yang C, Cheng L, Cheng M, et al. The establishment of a lung colonization assay for circulating tumor cell visualization in lung tissues. J Vis Exp. 2018;136:e56761. https://doi.org/10.3791/56761
20. Rask L, Fregil M, Høgdall E, Mitchelmore C, Eriksen J. Development of a metastatic fluorescent Lewis Lung carcinoma mouse model: Identification of mRNAs and microRNAs involved in tumor invasion. Gene. 2013;517(1):72–81. https://doi.org/10.1016/j.gene.2012.12.083.
21. Lee CB, Choi HG, Gurmessa SK, Jang IT, Kumar N, Jiang Z, et al. Enhancing antitumor immunity in Lewis lung cancer through plasma-treated medium-induced activation of dendritic cells. Cancer Cell Int. 2024;24:389. https://doi.org/10.1186/s12935-024-03569-x
22. Stankevicius V, Vasauskas G, Bulotiene D., Butkyte S, Jarmalaite S, Rotomskis R, et al. Gene and miRNA expression signature of Lewis lung carcinoma LLC1 cells in extracellular matrix enriched microenvironment. BMC Cancer. 2016;16:789. https://doi.org/10.1186/s12885-016-2825-9
23. Niu S-W, Wu C-H, Chen H-C, Yang C-J, Chang J-M, Chang EE, et al. Proteins secreted by lung cancer cells induce the onset of proteinuria via focal adhesion kinase signaling in mice. Lab Invest. 2023;103(8):100156. https://doi.org/10.1016/j.labinv.2023.100156
24. Pandey A, Vighetto V, Di Marzio N, Ferraro F, Hirsch M, Ferrante N, et al. Gold nanoparticles radio sensitize and reduce cell survival in Lewis lung carcinoma. Nanomaterials. 2020;10(9):1717. https://doi.org/10.3390/nano10091717
25. Pyaskovskaya ON, Dasyukevich OI, Kolesnik DL, Garmanchouk LV, Todor IN, Solyanik GI. Changes in VEGF level and tumor growth characteristics during lewis lung carcinoma progression towards cis-DDP resistance. Exp Oncol. 2007;29(3):197–202.
26. Posudievsky OYu, Khazieieva OA, Cherepanov VV, Dovbeshko GI, Shkavro AG, Koshechko VG, et al. Improved dispersant-free liquid exfoliation down to the graphene-like state of solvent-free mechanochemically delaminated bulk MoS_2. J Mater Chem C. 2013;1(39):6411–5. http://doi.org/10.1039/C3TC30856A
27. Yoneyama H, Sudo K, Leproux P, Couderc V, Inoko A, Kano H. Invited Article: CARS molecular fingerprinting using sub-100-ps microchip laser source with fiber amplifier. APL Photonics. 2018;3:092408. https://doi.org/10.1063/1.5027006
28. Gnatyuk O, Dovbeshko G, Dementjev A, Chernyakova K., Posudievsky O, Kupchak, et al. Spectroscopic and microscopic evidence of 2D boron nitride nanoflake interaction with doxorubicin. Opt Mater: X. 2024;22:100323. https://doi.org/10.1016/j.omx.2024.100323

ОПТИЧНА ТА ЕЛЕКТРОННА МІКРОСКОПІЯ ДЛЯ ВІЗУАЛІЗАЦІЇ МОДЕЛЬНИХ ЦИРКУЛЮЮЧИХ ПУХЛИННИХ КЛІТИН

М. Оленчук[1,*], Г. Монастирський[1], О. Гнатюк[1], А. Бойзен[2], Ч. Чжан[2], Г. Солянік[3], Д. Колесник[3], С. Карахім[4], Г. Довбешко[1]

[1]Відділ фізики біологічних систем, Інститут фізики НАН України, проспект Науки, 46, 03028 Київ, Україна;
[2]Відділ технологій охорони здоров'я, Технічний університет Данії, площа Ерстед, 345С, 2800, Кінгс-Лінгбю, Данія;
[3] Лабораторія молекулярних і клітинних механізмів метастазування, Інститут експериментальної патології, онкології і радіобіології ім. Р. Є. Кавецького НАН України, вул. Васильківська, 45, 03022 Київ, Україна;
[4]Відділ біохімії м'язів, Інститут біохімії ім. О.В. Палладіна НАН України, вул. Леонтовича, 9, 01030 Київ, Україна
* *e-mail: m.olenchuk@yahoo.com*

Надійшла до редакції 28 квітня 2025 р. Переглянута 25 травня 2025 р.
Прийнята до друку 25 травня 2025 р.

Актуальність. Мікроскопія є ключовим інструментом у біофізичних дослідженнях для візуалізації морфології, структури та динамічних процесів у живих клітинах. Залежно від конкретних задач застосовують різні методи оптичної та електронної мікроскопії, кожен з яких має свої переваги. Визначення особливостей будови цитоскелета, ядра, мембрани циркулюючих пухлинних клітин на моделі карциноми легені Льюїса (LLC) є важливою біофізичною та біологічною задачею, оскільки дозволить встановити мішені для протипухлинної та антиметастатичної терапії, а також дослідити механізми дії протипухлинних препаратів. Однак комплексне мультимодальне зображення таких клітин, особливо в умовах відсутності адгезії, залишається обмеженим у літературі через складність роботи з такими моделями.

Мета. Метою роботи було отримати зображення клітин карциноми легені Льюїса (LLC), вирощених в деадгезивних умовах, за допомогою різних методів мікроскопії. Завданням було оцінити

можливості кожного методу окремо та у поєднанні для візуалізації клітинної морфології, внутрішньоклітинної структури та взаємодії з наночастинками.

Матеріали та методи. Клітини LLC були отримані з Національного банку клітинних ліній та штамів пухлин ІЕПОР НАН України та культивувалися у середовищі RPMI-1640 в умовах деадгезивного росту. Візуалізацію проводили за допомогою інверсного оптичного мікроскопа (Euromex Oxion), флуоресцентної та конфокальної мікроскопії (Carl Zeiss LSM 510) з фарбуванням F-актину (Alexa Fluor 488-фалоїдіном) і клітинних ядер (Hoechst 33342), безміткової мікроскопії когерентного антистоксового розсіювання (Leica TCS SP8), а також скануючої електронної мікроскопії (TESCAN MIRA3 LMU). 2D-MoS_2 наночастинки, а також 2D-MoS_2 і доксорубіцин одночасно, були застосовані для дослідження опосередкованого маркування наночастинками клітин та поглинання клітинами.

Результат. У цій статті представлено порівняльний аналіз різних методів візуалізації культур клітин карциноми легені Льюїса (LLC), включаючи оптичні, флуоресцентні, конфокальні, КАРС і СЕМ мікроскопічні техніки. Флуоресцентна мікроскопія зі специфічними барвниками дала можливість зробити аналіз розмірів і морфології F-актинових волокон і показала, що ядра займають більшу частину деадгезивних клітин. Електронна мікроскопія виявила численні філоподії на поверхні клітин. КАРС виявив наявність ліпідних дроплетів в клітинах.

Висновки. Кожен із методів мікроскопії забезпечив унікальні та доповнюючі одна одну характеристики клітинної морфології, організації цитоскелета, вмісту ліпідів та структури мембрани. Наночастинки показали ефективність як подвійні агенти — маркери та носії препаратів. Вперше представлено докладне SEM-дослідження деадгезивних клітин LLC, що демонструє потенціал мультимодальної візуалізації для аналізу модельних циркулюючих пухлинних клітин.

КЛЮЧОВІ СЛОВА: модельні циркулюючі пухлинні клітини LLC; СЕМ; КАРС; конфокальна мікроскопія; наночастинки.